



HAL
open science

Investigation of europium retention on Callovo-Oxfordian clay rock (France) by laser ablation inductively coupled plasma mass spectrometry (LA-ICP-MS) and percolation experiments in microcells

Y. Hassan Loni, K. David, S. Ribet, Philippe Lach, Catherine Lerouge, B. Madé, C. Bailly, B. Grambow, Gilles F Montavon

► To cite this version:

Y. Hassan Loni, K. David, S. Ribet, Philippe Lach, Catherine Lerouge, et al.. Investigation of europium retention on Callovo-Oxfordian clay rock (France) by laser ablation inductively coupled plasma mass spectrometry (LA-ICP-MS) and percolation experiments in microcells. *Applied Clay Science*, 2021, 214, pp.106280. 10.1016/j.clay.2021.106280 . hal-03375306

HAL Id: hal-03375306

<https://hal.science/hal-03375306>

Submitted on 12 Oct 2021

HAL is a multi-disciplinary open access archive for the deposit and dissemination of scientific research documents, whether they are published or not. The documents may come from teaching and research institutions in France or abroad, or from public or private research centers.

L'archive ouverte pluridisciplinaire **HAL**, est destinée au dépôt et à la diffusion de documents scientifiques de niveau recherche, publiés ou non, émanant des établissements d'enseignement et de recherche français ou étrangers, des laboratoires publics ou privés.

1 **Investigation of Europium Retention on Callovo-Oxfordian Clay Rock (France) by**
2 **Laser Ablation Inductively Coupled Plasma Mass Spectrometry (LA-ICP-MS) and**
3 **percolation experiments in microcells.**

4
5 *Y. HASSAN LONI¹, K. DAVID¹, S. RIBET¹, P. LACH², C. LEROUGE², B. MADÉ³,*
6 *C. BAILLY¹, B. GRAMBOW¹ and G. MONTAVON^{1*}*

7 ¹Laboratoire SUBATECH, UMR 6457, IN2P3/CNRS/IMT Atlantique/Université de Nantes,
8 4, rue Alfred Kastler, BP 20722, 44307 Nantes cedex 3, France

9 ²BRGM, 3 avenue Claude Guillemin, F-45060 Orléans, France

10 ³Agence Nationale pour la gestion des Déchets Radioactifs (Andra), Direction Recherche &
11 Développement, 1/7 Rue Jean Monnet, 92298, Châtenay-Malabry Cedex, France

12 *Corresponding author: montavon@subatech.in2p3.fr

13 Phone: +33 251 85 84 20

14
15
16 **Abstract**

17 Clay-rock formations are under investigation in several countries as a potential host of
18 radioactive waste repositories. In order to assess the long-term safety of these concepts,
19 retention distribution data (Rd) are needed to describe the interaction between radionuclides
20 and natural rock. While Rd values obtained from batch-type experiments with dispersed
21 material are essential for the development of retention models, it is also important to generate
22 retention data under more realistic conditions, in particular with compact samples. Specifically,
23 the literature data on strongly retained radionuclides proves to be very scarce. The present study

24 focuses on the retention of europium at trace concentrations on clay samples extracted from the
25 Callovo-Oxfordian (COx) formation in France. Rd values obtained with compact COx samples
26 are assessed by a methodology coupling percolation experiments (in pressurized microcells),
27 performed using submillimeter-sized samples in thickness, and Laser Ablation Inductively
28 Coupled Plasma Mass Spectrometry measurements. The Rd found at trace concentrations under
29 non-transient conditions are high ($R_d > 10^4 \text{ mL g}^{-1}$) and in agreement with those recorded under
30 classical batch-type conditions or those deduced from the distribution of naturally-occurring Eu
31 between the pore water and the clay rock. They can be described by modeling with existing
32 sorption databases, considering an adsorption process only on the clay fraction. This was
33 validated by solid state LA-ICP-MS analyses of one of the Eu-spiked COx samples; the added
34 europium was found exclusively in the COx clay fraction.

35

36 **Keywords:** Retention, Clay rock, Europium, (LA)-ICP-MS, Percolation.

37

38

39 **I. Introduction**

40 The development of nuclear energy requires safe solutions for managing radioactive waste. The
41 worldwide consensus on the best way to protect human life and the environment is to dispose
42 of this radioactive waste in deep geological repositories. In France, the Callovo-Oxfordian
43 claystone formation (COx) is under investigation as a geological barrier to lower the fluxes
44 from the waste towards the geosphere, the hydrosphere and biosphere (ANDRA, 2005a; Sellin
45 and Leupin, 2013). This clay-rich formation, located in the Meuse/Haute-Marne site (Eastern
46 France), is characterized by low permeability, mineralogical homogeneity, high retention
47 capacities for radionuclides and little variation in other physicochemical properties (ANDRA,
48 2005b; Grambow, 2016).

49 To assess the long-term safety of this repository site, it is important to understand, characterize
50 and quantify the retention and transport properties of radionuclides in the host clay rock.
51 Retention processes, such as adsorption on mineral surfaces, precipitation as poorly soluble
52 pure solid phases, co-precipitation in the formation of minerals (neo-formation of a solid
53 solution) or incorporation into solid phases, can delay the radionuclides migration (Maes et al.,
54 2008) for a sufficient time to allow for radioactive decay.

55 "Safety analyses" generally consider adsorption processes (typically described by a list of
56 retention distribution data, or R_d values) leading to retardation of mass transfer. Scientifically,
57 for clayey rocks, these R_d values can be understood by cation exchange and surface
58 complexation reaction describing the concentration of labile species in rapid equilibrium with
59 a surface and a solution as a function of a number of environmental variables such as pH, pCO_2 ,
60 ionic strength, etc. The formation of these labile species can be described by thermodynamic
61 approaches. The modeling of radionuclide adsorption processes in the clay formation requires
62 numerous input parameters, many of which have been determined under laboratory conditions
63 with pure clay minerals. Experiments are carried out in batch-type mode in a state where the
64 solid is dispersed in large quantities of synthetic pore water for reasons of either duration or
65 ease of experimental implementation. The experiments are quite simple, relatively fast (a few
66 days) and able to be performed under a variety of well-controlled conditions; also, the data can
67 be used for assessing the dependency of retention parameters on the local mineralogy of the
68 host rock and its variation, on temperature, or on parameters describing the pore water
69 chemistry such as pH, pCO_2 , redox, other chemical species as aqueous silica or salinity
70 variations. However, it is essential to ensure that the adsorption parameters obtained on
71 dispersed materials are capable of describing adsorption processes on the actual compact
72 rock/pore water systems.

73 A relatively recent review (Miller and Wang, 2012) on the subject highlights various aspects
74 that can lead to differences depending on the state of compactness of the sample (surface-water
75 reactivity, accessibility of sorption sites, electrostatic considerations, double-layer overlapping,
76 etc.). For the case of Cs, Van Loon and Glaus (2008) critically examined the application of
77 thermodynamic models on highly compacted states whose ion hydration energies may differ
78 from those in the dispersed state. This important subject must therefore be treated for each class
79 of key radionuclides, which entails developing methods capable of determining retention
80 parameters for compact states.

81 In the ideal case, it would be possible to carry out batch-type retention experiments in a compact
82 system, i.e. waiting until a non-transient state is reached when the radionuclide concentration
83 in aqueous solution (in contact with the water-saturated porous system) and the radionuclide
84 concentration in pore water are equal. Under these conditions, the concentrations of
85 radionuclides both in pore water and retained on the solid surface can be measured, which
86 serves to calculate the distribution coefficient describing the retention (Rd) value. However,
87 achieving a non-transient state can take a long time due to the low permeability of the studied
88 compact clay materials. This approach appears to be feasible for highly compact states with
89 poorly or moderately retained radionuclides. A few number of studies can be found in the
90 literature for: I⁻ (Montavon et al., 2014), Cs⁺ (André et al., 2009; Chen et al., 2014b; Oscarson,
91 1994; Van Loon et al., 2009), Ni²⁺ (Montavon et al., 2020), and Sr²⁺ (Van Loon et al., 2005).
92 Overall, no clear evidence suggests that increasing clay compaction will lead to a fundamentally
93 different uptake of radionuclides.

94 For strongly sorbed ions/radionuclides, like trivalent metal ions, retention data are often
95 deduced from in-diffusion experiments, where information is derived from a transient state
96 (Descostes et al., 2017; Glaus et al., 2020; Kasar et al., 2016; Wang et al., 2004). The
97 information on metal retention is reliable provided species mobility has been adequately

98 described since compaction potentially affects both diffusive mass transfer and retention.
99 Therefore, it is fundamental to develop for strongly sorbed elements, in parallel with
100 transport/diffusion experiments, a set of methodologies yielding retention data in a non-
101 transient state (i.e. concentrations of radionuclides both in pore water and retained on the solid
102 surface can be measured), in order to assess the compaction effect on retention processes.

103 The objective of this work is to propose a non-transient method adapted to the retention study
104 of strongly sorbed elements on compact clay rock samples. It combines the use of pressurized
105 PEEK (Polyetheretherketone) micro cells, thereby limiting adsorption phenomena (Aertsens et
106 al., 2003) and accommodating submillimeter-thick samples, with a percolation mode to
107 accelerate transport so as to overcome the disadvantages of a long experimental duration by
108 using diffusion cells (Montavon et al., 2020 ; Chen et al., 2014b). After the experiment, the
109 strongly sorbed element is analyzed quantitatively on the (inlet) surface and in depth of the
110 compact sample by means of Laser Ablation Inductively Coupled Plasma Mass Spectrometry
111 (LA-ICP-MS). This technique turns out to be essential in the present context (due to its high
112 sensitivity and spatial resolution) to determining metal ion concentration in metal-spiked
113 compact samples as well as to assessing its distribution among the various mineral phases
114 present in the clay rock.

115 The methodology adopted in this study is applied to the Eu/CO_x system. Indeed, Eu is
116 considered to be a chemical homologue of certain trivalent actinides, such as Am or Cm, present
117 in radioactive waste (Kautenburger and Beck, 2010). Europium retention values published in
118 the literature are high and range from 5×10^4 to 10^5 L kg⁻¹ for trace concentrations, thus reflecting
119 a strong interaction with CO_x clay rock (ANDRA, 2005a; Descostes et al., 2017; Schott et al.,
120 2012). Retention data obtained in the compact state are compared herein with data measured in
121 the dispersed state and then discussed in light of both modeling results and a study of naturally-
122 occurring Eu in CO_x clay rock.

123

124 **II. Materials and methods**

125 A summary of the experiments carried out in the present study is given in Table 1.

126 Two types of experiments were performed as part of this study, namely: batch-type sorption
127 experiments on crushed COx samples in a dispersed state, and percolation experiments with
128 compact clay rock. All experiments were conducted at $T = 22 \pm 2^\circ\text{C}$ in the presence of a
129 synthetic pore water (SPW) whose simplified composition was based on geochemical modeling
130 exercises on *in situ* samples (Vinsot et al., 2008; Gaucher et al., 2009): $[\text{Na}^+] = 4.6 \times 10^{-2}$ M,
131 $[\text{K}^+] = 10^{-3}$ M, $[\text{Ca}^{2+}] = 7.4 \times 10^{-3}$ M, $[\text{Mg}^{2+}] = 6.7 \times 10^{-3}$ M, $[\text{Sr}^{2+}] = 2 \times 10^{-4}$ M, $[\text{Cl}^-] = 4.1 \times 10^{-2}$
132 M, $[\text{SO}_4^{2-}] = 1.6 \times 10^{-2}$ M, inorganic carbon = 4.5×10^{-3} M (in equilibrium with calcite), and pH
133 = 7.3. Inorganic carbon was controlled by use a N_2/CO_2 (1%) gas mixture ($P_{\text{CO}_2} = 10^{-2}$ atm)
134 either in a glove box (batch-type experiments) or by bubbling inlet solution (percolation
135 experiments).

136 All solutions were prepared with ultra-pure deionized water (18.2 M Ω .cm) and with
137 commercially available chemical products of analytical grade or superior. For the SPW
138 preparation, analytical grade $\geq 99\%$ ACS reagents (NaCl, $\text{Na}_2\text{SO}_4 \cdot 10\text{H}_2\text{O}$, $\text{CaCl}_2 \cdot 2\text{H}_2\text{O}$, MgCl_2
139 $\cdot 6\text{H}_2\text{O}$, NaHCO₃, KCl) and $\text{SrCl}_2 \cdot 6\text{H}_2\text{O}$ product from Sigma Aldrich (99.995% trace metals
140 basis) were used.

141 A stock solution of EuCl_3 (99.99% trace metals basis, Sigma Aldrich) was used to obtain initial
142 concentrations of Eu between 1.9×10^{-9} and 1×10^{-7} mol L⁻¹. Sources of ¹⁵²Eu (Eckert & Ziegler)
143 in 0.5M HCl (with 10 $\mu\text{g/g}$ of carrier) and HTO (Eckert & Ziegler) served as radioactive tracers.

144

145 **II.1 COx samples**

146 The CO_x samples used were obtained from the Meuse/Haute-Marne Underground Laboratory
147 (depth: \approx 500 m) located in the eastern part of the Paris basin. They originated from boreholes
148 drilled by Andra (French Radioactive Waste Management Agency). The mineralogical
149 composition and proportions of the major phases have been extensively described in Gaucher
150 et al. (2004), ANDRA (2005b) and Lerouge et al. (2011). This composition mainly consists of
151 phyllosilicates (40-60 wt%, mainly illite and mixed layer illite/smectite, kaolinite and chlorite),
152 carbonates (15-45 wt%, mainly calcite and dolomite), tectosilicates (10-40 wt%, mainly quartz
153 and feldspars) and minority phases such as sulfides (0-3 wt%, mainly pyrite) and natural organic
154 matter (0.5-1 wt%).

155 After drilling, the samples were conditioned in airtight aluminum foil filled with nitrogen,
156 transported to the laboratory and then stored until their opening in a N₂/CO₂ (1%) glove box.

157 For the measurement of natural Eu concentrations in the pore water of CO_x, seepage water from
158 the Callovo-Oxfordian clay-rich rock was collected from borehole GIS1002 in Andra's
159 Meuse/Haute-Marne underground research laboratory. This 16-m long horizontal borehole was
160 drilled at a depth of 490 m in the clay-rich layer. The water sample analyzed was collected 10
161 years after the borehole began to produce water (Grangeon et al., 2015).

162 163 **II.2 Batch-type experiments**

164 Europium retention on CO_x was investigated by means of batch-type experiments as a function
165 of Eu concentration at a fixed solid/liquid (S/L) ratio (0.5 g L⁻¹). An appropriate amount of CO_x
166 powder (grain size < 200 μ m) was dispersed in SPW in 35-mL Nalgene[®] Polypropylene
167 Copolymer (PPCO) centrifugation tubes. After one day of mechanical agitation to equilibrate
168 the "SPW/CO_x/atmosphere" system, Eu was added to the suspension. The Eu concentration
169 domain was chosen (by modeling) so as to avoid any precipitation of Eu hydroxide or carbonate
170 solid phases (see Table 1). Preliminary experiments showed that a contact time of at least 4

171 days was necessary to reach sorption equilibrium, as indicated by constant Eu concentrations
172 in the aqueous phase, within the uncertainties, as a function of the time (data not shown). The
173 supernatant was recovered using 0.22- μm surfactant-free cellulose acetate filters for Eu
174 analysis.

175 The solid/liquid distribution coefficient, R_d (in L kg^{-1}), and associated error (Err_{R_d}) were
176 determined according to the following equations:

$$177 \quad R_d = \frac{C_s}{C_{eq}} = \frac{C_0 - C_{eq}}{C_{eq}} \times \frac{V}{m} \quad (1)$$

178 where C_s (mol g^{-1}), C_0 (mol L^{-1}), C_{eq} (mol L^{-1}), V (L) and m (kg) are respectively: the amount
179 of Eu adsorbed onto the solid, the initial and equilibrium aqueous concentrations of Eu, the
180 volume of the aqueous solution, and the mass of the COx powder.

181 the associated error is calculated according to the equation:

$$182 \quad Err_{R_d} = \sqrt{\left(\frac{V}{m} \frac{C_0}{C_{eq}}\right)^2 \times \left(\left(\frac{Err_{C_0}}{C_0}\right)^2 + \left(\frac{Err_{C_{eq}}}{C_{eq}}\right)^2\right) + R_d^2 \times \left(\frac{Err_{V/m}}{V/m}\right)^2} \quad (2)$$

183 with Err_{C_0} , $Err_{C_{eq}}$ and $Err_{V/m}$ being the uncertainties linked to C_0 , C_{eq} and V/m , respectively.

184 In parallel to the sorption experiments, "blanks" were systematically performed with SPW in
185 the presence of Eu without COx to quantify the total Eu content (C_0); no significant adsorption
186 of Eu on either the tube surfaces or the filters under the experimental conditions of this study
187 was observed (<5%).

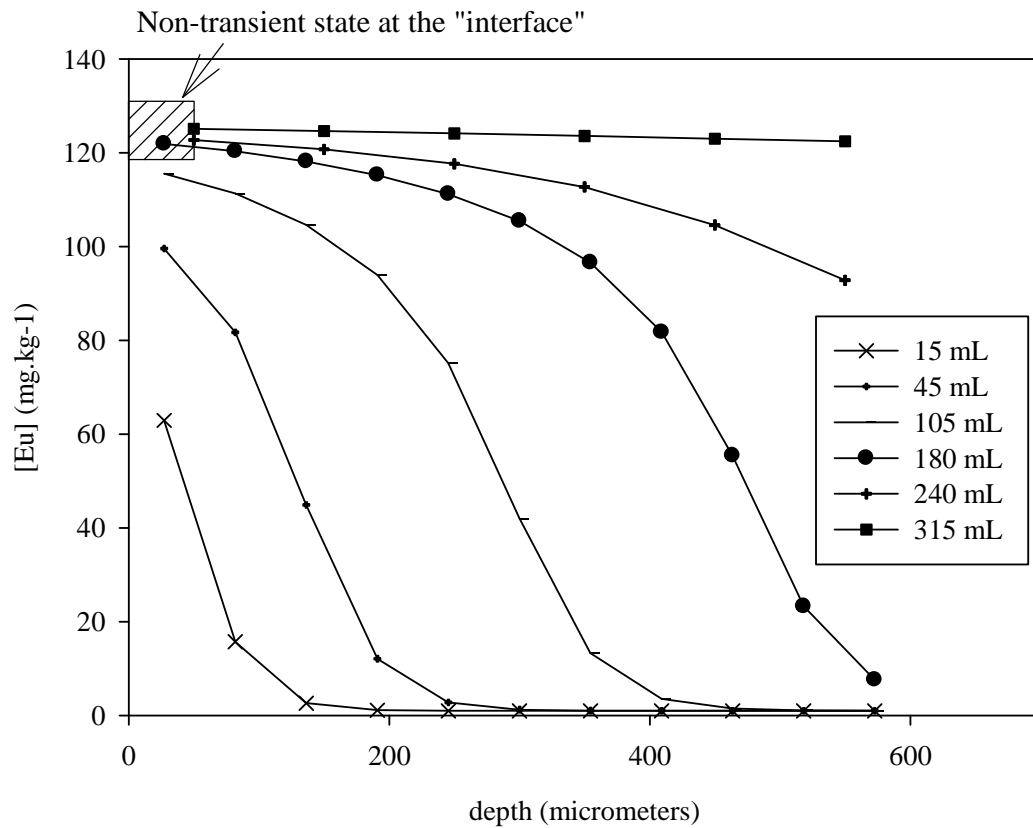
188 Each point on the isotherm corresponds to the result of a single test.

189 **II.3 Percolation experiments**

190 *II.3.1 Experimental strategy*

191 The methodology applied for percolation experiments involves injecting the element of interest
192 (at a given concentration) under pressure through the compact clay medium saturated with
193 synthetic pore water (in equilibrium with the phases present) (see Table 1 for more details).
194 We recall that the objective is to obtain a non- transient state, i.e. that element concentration at
195 the output of the assembly is equal to the injected concentration. Since the solution
196 concentration is known, a value for R_d can be calculated by determining the concentration of
197 the element in the adsorbent phase, here CO_x . It is also worth mentioning here that the transient
198 /non- transient state is not related to the notion of the establishment of an equilibrium state
199 between the soluble and adsorbed fractions of the element. This equilibrium state, which allows
200 the application of thermodynamic models, is dependent on the rate of adsorption of the element
201 onto the material. Such a state of equilibrium for the adsorption process is assumed with clays,
202 whether we are working under transient or non-transient conditions.

203 If we come back to our percolation experiences, a non-transient state can be obtained for
204 Cs/CO_x (Chen et al., 2014b) or Ni/CO_x (Montavon et al., 2020) systems. For the case of Eu ,
205 which is a strongly retained element, this condition is more complicated to achieve. By way of
206 illustration, Fig. 1 shows initial simulations that were carried out with literature data, i.e. a value
207 of R_d around $10^5 L kg^{-1}$ (ANDRA, 2005a; Descostes et al., 2017; Schott et al., 2012). It can be
208 seen that the non-transient state is reached after about 6 years of experiments, even though the
209 work is being carried out in advective mode with submillimeter-sized samples in thickness (Fig.
210 1).



211

212 *Fig.1: Simulations of Eu profile evolution in a compact COx sample vs. depth for different percolation*
 213 *volumes (for roughly 6 years of experiment). Flow rate: 0.15 mL day⁻¹; sample thickness: 0.6 mm;*
 214 *[Eu]_{injected}=8.2×10⁻⁸ M; Rd=7.8×10⁴ L kg⁻¹. Information for the simulation is available in Table A1.*

215

216 In order to limit the experimental time (i.e. a few months), the strategy adopted in our study
 217 sought a non-transient state at the inlet surface, or at least within the first few micrometers. By
 218 measuring Eu concentration at the surface by LA-ICP-MS ([Eu]_{clay,COx}, in mol per mass of
 219 COx) with a known Eu concentration in the injection loop ([Eu]_{injected}, in mol per volume of
 220 SPW) it is then be possible to calculate a Rd value:

$$221 \quad Rd = \frac{[Eu]_{clay,COx}}{[Eu]_{injected}} \quad (3)$$

222 The amount of spiked Eu in the COx was systematically corrected from the amount of Eu
 223 naturally present.

224 The retention parameter obtained can subsequently be used as a fixed value in an attempt to
225 reproduce the Eu “percolation depth profiles” using a reactive transport model (see part II.5).

226
227 *II.3.2 CO_x clay rock samples*

228 Naturally highly compact samples were used (bulk density of $\sim 2.3 \text{ g cm}^{-3}$). The sample
229 preparation methodology was adapted from Montavon et al. (2020, 2014). First, a 1-cm
230 diameter piece (several centimeters long) was manufactured through core drilling; next, a lathe
231 (Caseneuve HB55) was used to obtain a diameter of $4.99 \pm 0.02 \text{ mm}$. Lastly, the piece was
232 fastened onto a support and cut into slices (thickness: $0.5 - 0.8 \pm 0.05 \text{ mm}$) by means of a
233 precision diamond wire saw (Escil[®] W3032; wire diameter = 0.3 mm). These steps were
234 performed under air, but the potential superficial oxidation of the minerals was minimized by
235 using a nitrogen flow around the rock samples. Note that a possible partial oxidation of the
236 sample will not have a direct effect on the retention of Eu: Eu is not a redox sensitive element
237 and neither is the clay fraction of CO_x.

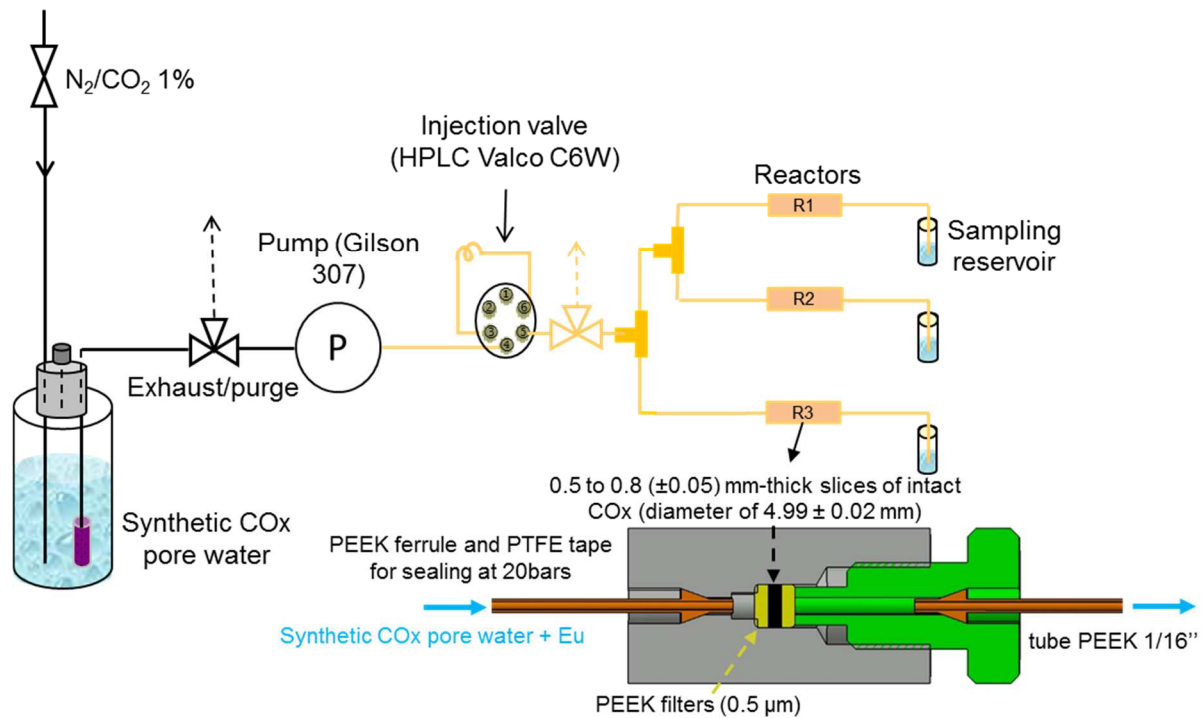
238 The dry bulk densities of the pellets output ranged from 2.18 to 2.28 g cm^{-3} .

239 The samples were initially qualitatively characterized by Optical Microscopy (Olympus BH2)
240 and Scanning Electron Microscopy (Tescan Mira 3 XMU) (SEM) in order to select the "right
241 candidates" (Fig. A1). The aim of this initial characterization was to discard CO_x pellets with
242 cracks or those with crumbled edges and then select only those pellets characterized by a
243 homogeneous distribution of CO_x mineral phases (compared to average compositions).

244 *II.3.3 Percolation experiment set-up*

245 The percolation experiment set-up is presented in Figure 2. The reactors have been designed to
246 ensure total system tightness and allow for total sample recovery once the experiment has been
247 completed. The material used to make the reactors and the capillary tubes are made of PEEK

248 in order to avoid or limit Eu adsorption phenomena (Molera and Eriksen, 2002). An assembly
 249 of three reactors R1, R2 and R3 connected in parallel was installed for the purpose of
 250 performing several experiments with just a single pump. Each part of the percolation cell was
 251 cleaned successively with HNO₃ 5% (v/v), Milli-Q water and Normapur 96% ethanol before
 252 drying (in the glove box) and use.



253

254 *Fig. 2: The percolation experiment set-up*

255 Once the samples had been inserted into the cells (between two PEEK filters), they were first
 256 hydrated and equilibrated with SPW. Sample hydration proceeded in stages, initially at low
 257 pressure (1 bar) for 3 days before pressure was gradually increased to 20 bar so as to determine
 258 the permeability and verify the applicability of Darcy's Law (Fig. A2). Average flows were 158
 259 ± 10, 132 ± 7 and 101 ± 9 mg d⁻¹ for R1, R2 and R3, respectively. In order to maintain the pH
 260 and carbonate concentration of the SPW constant throughout the duration of the experiment, a
 261 bubbling with a N₂/CO₂ (1%) gas mixture was carried out for at least 15 min twice a week. In
 262 the meantime, pH was measured from time to time in the sampling reservoir to ensure that the

263 system remained in equilibrium. SPW with Eu at $(8.8 \pm 0.9) \times 10^{-8} \text{ mol L}^{-1}$ was injected into the
264 percolation cell at a constant pressure of 20 bar. In order to avoid Eu adsorption on the pump
265 head, the solution was injected via a 7.85 mL injection loop (made of PEEK) (Fig. 2). In other
266 words, the Eu-free SPW solution in the vessel in Fig. 2 “pushes” the Eu-doped SPW solution
267 (present in the loop) into the compacted COx pellet. Note that the loops were changed in time
268 to ensure a constant supply in Eu concentration in the COx. The outlet solution was analyzed
269 regularly to both control the possible presence of Eu and measure pH values and alkalinity.

270 Europium solution percolation through samples R1, R2 and R3 was stopped after 174, 365 and
271 694 days, respectively. The collected solution volumes were of 25, 49 and 58 mL for R1, R2
272 and R3, respectively. Compact COx samples extracted from R1 and R2 reactors were recovered
273 and cut in half using a sterilized scalpel (washed in AnalaR Normapur® 96% vol. ethanol
274 (VWR BDH Prolabo) and 5% (v/v) Teflon distilled nitric acid and then rinsed with Milli-Q
275 water).

276 The Eu “percolation depth profiles” were obtained by analyzing the side of the pellet in depth
277 (from the surface in contact with the input solution to the end of the pellet from which the
278 solution was recovered).

279 Each half-sample piece was fastened onto a thin petrographic plate with a double-sided
280 adhesive disc for the Eu microanalysis of sample surface and depth profile by means of Laser
281 Ablation Inductively Coupled Plasma Mass Spectrometry. For R1 and R2 samples, Eu
282 concentrations were measured in relation to the mass of COx ablated. For R3, the analysis was
283 concentrated on the clay fraction of the COx.

284 Results were compared with the distribution of Eu naturally present.

285

286

287

288 *Table 1: Summary of the experimental conditions in effect during this study*

Sample	Type of sample	Type of experiment	Focus	Contact time (days)	Figure(s)
EST45989 (R1)	Compact	Spiked by percolation	Eu concentration at the surf ^{*ace} and as a function of depth. $[\text{Eu}]_{\text{injected}} = (2.4 - 2.7) \times 10^{-8} \text{ mol L}^{-1*}$	174	5, 6, A1-2, 5
EST45989 (R2)			365	5, 6, A1-2, 5	
EST45989 (R3)			Eu in clay fraction at the surface. $[\text{Eu}]_{\text{injected}} = 9.1 \times 10^{-8} \text{ mol L}^{-1*}$	694	5, A1-2, A6
EST51779	Crushed	Spiked in the dispersed state	Rd measurement: $[\text{Eu}]_0 = 1.9 \times 10^{-9} - 10^{-6} \text{ mol L}^{-1}$ (experiments with the radioactive tracer)	4	3
EST51779	Compact	Naturally-occurring Eu	Eu distribution in COx mineral phases	-	3, 4, A1, A3

289 * concentrations measured at the end of the experiment; the initial concentration injected was
290 $(8.8 \pm 0.9) \times 10^{-8} \text{ mol L}^{-1}$

291 **II.4 Analytical techniques**

292 The SPW composition was measured by ionic chromatography (Dionex ICS1000). A pH
293 electrode (Inlab), freshly calibrated with standard pH buffers (pH 4, 7 and 10, Fisher), was used
294 to measure pH values. The alkalinity was determined by colorimetric analysis using
295 Bromocresol Green-Methyl Red Indicator Powder Pillow as color indicator and a Digital
296 Titrator (Hach method 8203) with a digital titrator cartridges containing 0.16 N of H₂SO₄.
297 Analyses of radioactive Eu (¹⁵²Eu) in solution (8 mL) were performed by liquid scintillation
298 counting with a Packard TriCarb 3170 TR in adding an Ultima Gold LLT[®] (Perkin Elmer)
299 scintillation cocktail (12 mL).

300 Direct analyses of Eu concentration in COx samples were conducted by LA-ICP-MS on thin
301 samples polished under dry conditions in order to avoid any contamination or loss of trace
302 element with reagents. Analyses of both natural (surface Eu concentration) and compact spiked
303 COx R1 and R2 (depth profile and surface Eu concentration) samples were measured by LA-
304 HR-ICP-MS at the SUBATECH Laboratory. Analyses of Eu concentration in the clay fraction
305 of the compact Eu-spiked COx sample from the R3 reactor were performed by LA-Q
306 (quadrupole)-ICP-MS at the BRGM (French Geological Survey) facility.

307 In order to identify the phases at the origin of Eu retention (Eu-COx sample from R3, natural
308 COx sample), mineral phases (pyrite, calcite and clay fractions) were first characterized using
309 an Olympus BH2 optical microscope (Fig. A3) and then localized by diamond strapping to
310 assist with the analyses.

311 Note that the ability of the LA-ICP-MS technique to accurately quantify the amount of Eu was
312 assessed with the natural sample by comparison with the amount measured in solution after
313 sample acid digestion (Fig. A6).

314

315 *II.4.1 LA-HR-ICP-MS*

316 Micro-analyses of Eu in the natural COx or Eu-spiked COx (R1 and R2) samples were
317 undertaken using a Nd-YAG UP213 laser system (NewWave Research) coupled with the
318 Element XR single collector high resolution ICP-MS (Thermo Scientific). The HR-ICP-MS
319 was synchronized to the laser ablation device in external trigger mode. The laser system was
320 equipped with a standard ablation cell (V=30 ml) mounted on a motorized xyz stage with sub-
321 micron resolution for sample movement. The ablated material was removed from the sample
322 chamber by helium carrier gas, then mixed with argon gas and directly introduced into the hot
323 plasma of the HR-ICP-MS instrument. Operating conditions have been detailed elsewhere
324 (Hassan Loni et al., 2019). The Eu concentration was determined by external calibration using
325 two standard reference materials, i.e. the NIST 610 synthetic glass with [Eu] (mg kg^{-1}) = $447 \pm$
326 10 ($k=2$) and the matrix-matched NIST 679 brick clay with [Eu] (mg kg^{-1}) = 1.9 ± 0.2 ($k=2$)
327 prepared in a compacted disc-shaped pellet. The quantification procedure was carried out
328 according to two distinct approaches, namely: internal standardization with a major element of
329 known concentration used as internal standard, and the 100% oxide normalization in applying
330 the total matrix (58 elements) as an internal standard (Lin et al., 2016; Liu et al., 2008; Šelih
331 and Van Elteren, 2011; Van Elteren et al., 2009).

332 The Eu depth profiles of R1 and R2 COx samples were analyzed in either line scan or single-
 333 spot ablation modes according to the 100% oxide (w/w) normalization strategy. The laser was
 334 operated at a pulse repetition rate of 10 Hz, with an output energy of 50% (≈ 0.5 mJ) and beam
 335 diameter of 65 μm (line scan) or 50 μm (single spot). A total analysis time of 3 min was defined
 336 for the line ablation mode (2 min for the single-spot mode), including 2.25 min (or 1 min) and
 337 1.7 min (or 1 min) for laser ablation sample and gas blank measurements, respectively.

338 Micro-analyses of Eu in polished thin sections of natural COx mineral phases were performed
 339 by both external calibration and internal standardization (^{29}Si or ^{27}Al for clay fraction, ^{42}Ca for
 340 calcite and ^{57}Fe for pyrite). The laser settings were as follows: output energy = 50% (≈ 0.5 mJ),
 341 frequency = 10 Hz, and beam diameter = 55 μm . Each optimal laser analysis lasted 2 min,
 342 encompassing 30 s to 60 s of laser sample ablation (depending on the beam length, with beam
 343 diameter = 55 μm) and 60 s of background measurement. The laser beam length was adapted
 344 to the size of the mineral phase being analyzed.

345 All time-resolved raw data were exported in ASCII or FIN2 format and processed offline by
 346 in-house subroutines written in VBA language for Microsoft Excel 2010TM. The average gas
 347 blank signal intensities for all elements were calculated and then subtracted from the signal
 348 intensities measured during the standard and sample ablation step. A signal drift correction was
 349 applied with a linear interpolation over time by using normalized ^{151}Eu signal intensities from
 350 the bracketing standard reference materials. A two-sigma rejection test of outliers was applied
 351 to all normalized sample Eu signal intensities. The Eu concentration of each analysis were
 352 calculated from the following equations:

$$353 \quad C_{\text{SMP}}^i(\text{norm}) = 100 \times \frac{\hat{I}_{N_x}^{i,\text{SMP}}}{\frac{[\hat{I}_{N_2}^{i,\text{STD}} \times (N_x - N_1) + \hat{I}_{N_1}^{i,\text{STD}} \times (N_2 - N_x)]}{(N_2 - N_1)}} \times \frac{C_{\text{STD}}^i}{\sum_{i=1}^n C_{\text{SMP}}^i(\text{unnorm})} \quad (4)$$

$$354 \quad \text{with: } C_{\text{SMP}}^i(\text{unnorm}) = \frac{\hat{I}_{\text{SMP}}^i}{\hat{I}_{\text{STD}}^i / C_{\text{STD}}^i}$$

355 where \hat{I}_{SMP}^i , \hat{I}_{STD}^i and C_{STD}^i are the signal intensity (in cps) for each of the sample-containing
356 elemental oxides i (1 to n), the signal intensity and the elemental oxide concentration i (in %
357 (w/w)) of elemental oxide i in NIST 610, respectively. N_1 , N_2 and N_x denote the analysis
358 numbers in the sequence.

359

360 *II.4.2 LA-ICP-Q-MS*

361 The microanalysis of Eu in the clay fraction of the spiked COx sample (R3) was performed by
362 a UV Laser-Ablation micro sampler CETAC[®] Excite (193 nm) coupled with a
363 ThermoScientific[®] X series II quadrupole plasma mass spectrometer, according to the laser
364 configuration set forth by (Monnier et al., 2018). The analytical protocol involved combinations
365 of ²⁷Al, ²⁹Si, ⁴⁴Ca and ¹⁵¹Eu analyses. Ablation spots 35 μm in diameter were introduced at an
366 8-Hz frequency with an energy of $\approx 2 \text{ J cm}^{-2}$. The analysis time for each spot was 60 s, including
367 20 s of background measurement with the laser off and 40 s of analysis time with the laser on.
368 The Eu concentration was calibrated against the external standard NIST 612, the internal
369 standard of the Si value for clay minerals and the Ca value for carbonates.

370 **II.5 Reactive transport and sorption models**

371 All calculations were carried out using the PhreeqC code (Version 3.3) (Parkhurst and Appelo,
372 2013) using the Davies Equation (Davies, 1964) to account for the ionic strength correction of
373 solutes.

374 Reactions occurring in the aqueous phase as well as saturation states with respect to solid phases
375 were calculated using the thermodynamic database ThermoChimie v9b (Giffaut et al., 2014)
376 (Grivé et al., 2015; <https://www.thermochimie-tdb.com/>) (Table A2).

377 To model Eu adsorption, two assumptions were introduced: 1) the clay fraction governs Eu
378 retention in assuming that illite and interstratified IS were the reactive phases with IS-combined
379 illite (50% in weight) and smectite (50% in weight) properties (Chen et al., 2014a; Grangeon et
380 al., 2015; Tournassat et al., 2008); and 2) the additivity (Davis et al., 1998) approach is valid,
381 whereby the models developed for the clay model phases illite and montmorillonite (smectite)
382 can be directly applied to the COx material without considering additional reactive phases or
383 modifying interaction parameters in the complex multi-mineral assemblage including mixed
384 layer illite-smectite (IS). The 2-site protolysis, non-electrostatic surface complexation and
385 cation exchange model (2 SPNE SC/CE) (Bradbury and Baeyens, 2011) was implemented for
386 the COx clay rock. According to the 2 SPNE SC/CE model, the surface complexation
387 phenomenon is controlled by both weak (i.e. high quantity, limited affinity) and strong (low
388 quantity, high affinity) sites. No competitive effect was considered between Eu and other trace
389 metals at the adsorption sites (Bradbury and Baeyens, 2011; Marques Fernandes et al., 2015).
390 Unless otherwise indicated, calculations were performed for COx with the lower and upper clay
391 content limits. This approach introduces the greatest error sources, while other uncertainties
392 associated with model parameters were not considered (Table A3). Considering in the clay-rich
393 zone the variation in clay (40-60 wt%), the variation in illite and I/S, and a percentage of 55%
394 of smectite in I/S (Chen et al., 2014a; Gaucher et al., 2004), range of 20–44% and 9–18% for
395 illite and montmorillonite respectively were used in the calculations.

396 For the percolation experiments, the 1D coupled chemical/transport model (reactive code)
397 implemented in phreeqC was used. For the modeling step, the two filters in PEEK, with a
398 porosity of 9.4 vol%, were taken into account, along with the length of capillary tubes at both
399 the cell inlet and outlet. Dead volumes were estimated by simulating HTO injection through the
400 samples (Fig. A5). Note that results indicate the absence of dilution in the HTO solution injected
401 through the capillary loop.

402 The relative magnitudes of advection and dispersion are characterized by the Peclet number, as
403 defined by:

$$404 \quad Pe = vL / (D_p + \lambda v) \quad (5)$$

405 where L is the sample length (m), v the pore water velocity (m s^{-1}), D_p the pore diffusion
406 coefficient ($\text{m}^2 \text{s}^{-1}$), and λ the dispersivity (m). $D_p + \lambda v$ represents the dispersion coefficient.

407 The D_p value was set at $1.5 \cdot 10^{-11} \text{ m}^2 \text{ s}^{-1}$ (Altmann et al., 2014). Peclet numbers were estimated
408 in the range of 2 - 4 for compact CO_x samples, thus indicating the predominance of the
409 advection mode over the diffusion mode.

410 The column hydrodynamic characteristics required for modeling (porosity, samples
411 dimension,....), as well as the data used for describing Eu adsorption, can be found in Tables
412 A1-A3.

413

414 **III. Results**

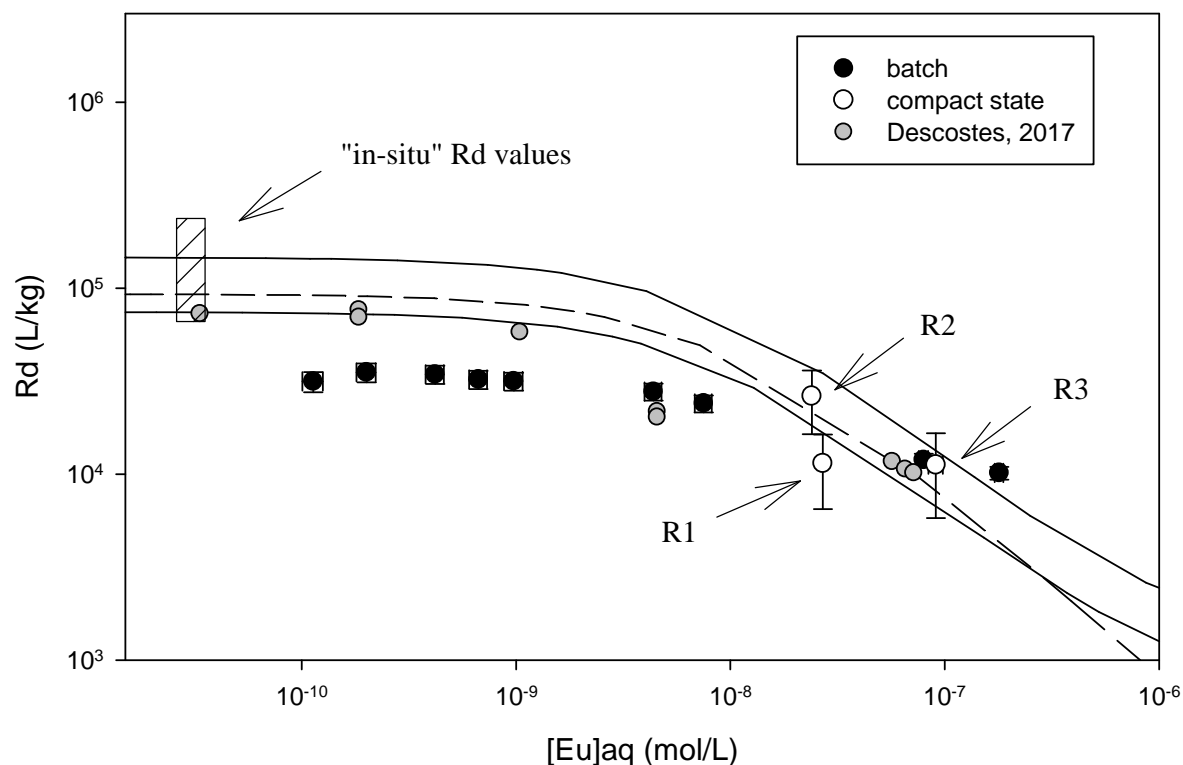
415 **III.1 Batch-type experiments in the CO_x dispersed state**

416 Figure 3 presents the sorption isotherm of Eu on CO_x as well as those published for the Eu/CO_x
417 system by Descostes et al. (2017) under similar conditions. The pH and alkalinity values of the
418 supernatant were: 7.3 ± 0.1 and $2.64 \pm 0.14 \text{ meq L}^{-1}$, respectively. Europium sorption is constant
419 at the lowest concentration, with R_d values around $(3.5 \pm 0.5) \times 10^4 \text{ L kg}^{-1}$. These values are of
420 the same order of magnitude as those given for similar experimental conditions by both García-
421 Gutiérrez et al. (2009) ($> 3.8 \times 10^4 \text{ L kg}^{-1}$) and ANDRA (2005b) ($\approx 5 \times 10^4 \text{ L kg}^{-1}$) yet lower than
422 that obtained by Descostes et al. (2017) ($\approx 1 \times 10^5 \text{ L kg}^{-1}$).

423 Rd values then decrease to approx. 10^4 L kg^{-1} at the highest concentration studied ($\approx 2 \times 10^{-7} \text{ mol}$
424 L^{-1} for aqueous Eu concentration). Under these conditions, our data are consistent with those of
425 Descostes et al. (2017).

426 The simulation results are represented by the solid lines for the lower and upper clay fraction
427 limits. Under the experimental conditions of this study, Eu speciation in solution is dominated
428 by carbonate complexes. Carbonate ions also appear to be important in describing the
429 adsorption of Eu; at the lowest Eu concentrations, adsorption is controlled by the formation of
430 two carbonate surface complexes with strong sites ($\text{sOEu}(\text{CO}_3)$ and sOEuOHCO_3^- , Table A2).
431 In this range, the model overestimates our retention data by about one order of magnitude. For
432 the highest concentrations studied, i.e. the zone where the percolation experiments were carried
433 out, the simulation and experimental results are consistent. Under these conditions, the
434 contribution of weak sites to retention becomes significant ($\approx 15\%$).

435 Given this study's objective, no further work has been carried out in search of an explanation
436 for this discrepancies observed at the lowest Eu concentrations.



438

439 *Fig. 3: Eu adsorption onto a COx sample in the presence of SPW and modeling results. (●) Batch-type*
 440 *experiments; (○) Percolation experiments in the compact state (R1, R2 and R3). (▲) Data from*
 441 *Descostes et al. (2017). Solid lines depict simulations performed for the lower and upper clay fraction*
 442 *limits. The dashed line represents the contribution of the two carbonate surface complexes ($s\text{OEu}(\text{CO}_3)$*
 443 *and $s\text{OEuOHCO}_3^-$) to the overall retention for the mean COx clay fraction. Simulation details are given*
 444 *in Tables A2 and A3.*

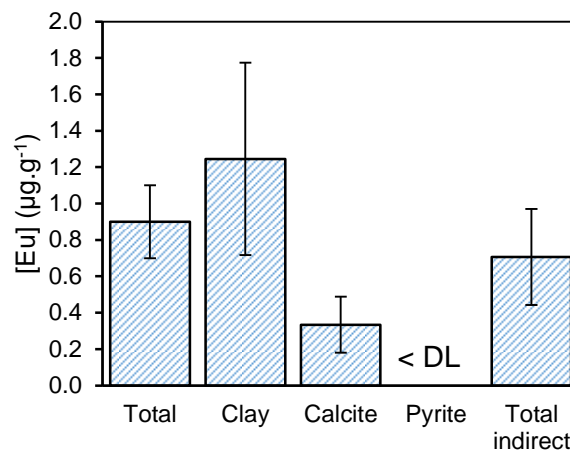
445

446 III.2 Naturally-occurring Eu

447 The two analytical approaches (the direct analysis on the solid vs. the analysis of the solution,
 448 after digestion) yield similar values, i.e. an Eu concentration of $0.9 \pm 0.2 \mu\text{g g}^{-1}$. As expected,
 449 Eu is present at trace levels in the clay formation; to the best of our knowledge, this is the first
 450 reported value for Eu.

451 The various constituent mineral phases (i.e. clay, calcite, pyrite) were analyzed by means of
 452 LA-HR-ICP-MS in order to assess the distribution of naturally-occurring Eu in the COx. These
 453 mineral phases were chosen for their recognized ability to trap metals through various retention

454 processes (Descostes et al., 2017); results are provided in Figure 4. The mass balance
 455 calculations performed from the direct analyses carried out on individual phases did appear to
 456 be consistent, given the uncertainties present, with the total quantity of Eu in the sample. The
 457 main mineral phases with more affinity to Eu have therefore been identified.



458

459 *Fig. 4: Distribution of naturally-occurring Europium studied by LA-HR-ICP-MS (the number of*
 460 *analyses are 10, 5 and 3 for clay, calcite and pyrite, respectively). "Total indirect" corresponds to the*
 461 *Eu content in the COx determined by summing the Eu concentrations measured in the individual phases*
 462 *(normalized to their % in COx). (DL = Detection Limit)*

463

464 Europium is mainly present in the clay fraction ($1.2 \pm 0.5 \mu\text{g}$ per g of clay fraction) and
 465 contributes to about 70% of the inventory ($0.9 \mu\text{g}$ per g of COx) if the average clay content
 466 found in the COx (≈ 50 wt%) is taken into account. For calcite (≈ 25 wt%), the average Eu
 467 concentration obtained ($0.33 \pm 0.15 \mu\text{g}$ per g of calcite) is less than that determined in the clay
 468 phase. The contribution of calcite to average Eu concentration in the COx has been estimated
 469 at roughly 10%. No Eu was detected in the pyrite phase (i.e. $< \text{DL} = 0.001 \mu\text{g g}^{-1}$). These results
 470 indicate that the clay fraction is the main "reservoir" for Eu in the COx.

471 In assuming that the clay fraction controls adsorption (i.e. the starting hypothesis of the
 472 adsorption model), it is then possible to revert to Rd values as long as the concentration of Eu
 473 in the pore water remains known. A value of $(3.0 \pm 0.4) \times 10^{-11} \text{ mol L}^{-1}$ was experimentally
 474 measured by means of HR-ICP-MS for the GIS1002 borehole. With these concentrations in

475 water and clay fraction, a range of Rd values can be estimated from around $6 \cdot 10^4$ to $2 \cdot 10^5$ L kg⁻¹
476 ¹ (hatched area in Figure 3).

477

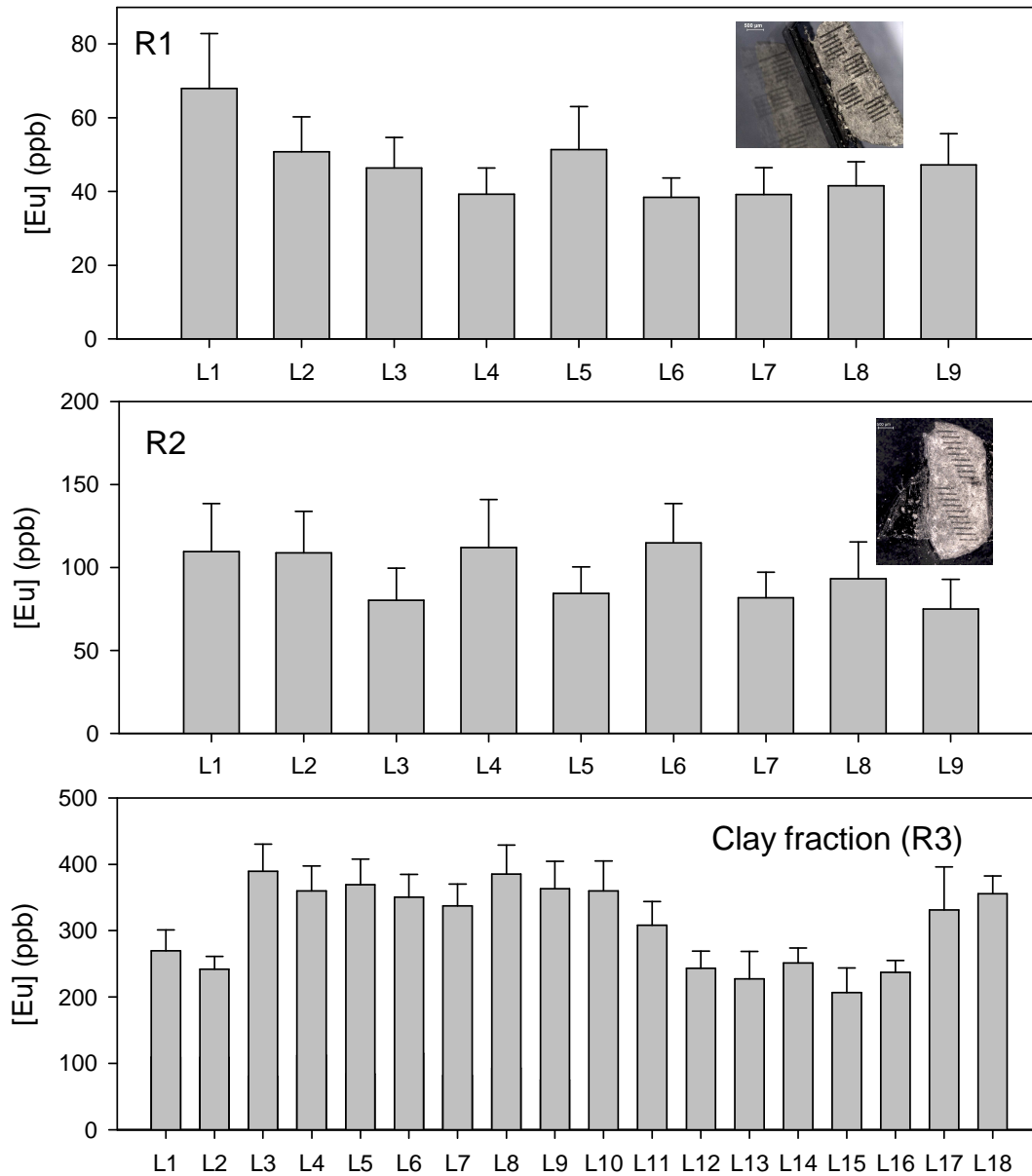
478 **III.3 Percolation experiments**

479 For all samples, the linearity obtained between flow rate and pressure gradient serves to validate
480 the applicability of Darcy's Law under our experimental conditions. The measured permeability
481 values varied between 3.3×10^{-13} and 4.2×10^{-13} m s⁻¹ (Fig. A2); these values are in good
482 agreement with data for compact rock found in the literature (ANDRA, 2005b; Vinsot et al.,
483 2008). The CO_x/SPW equilibrium was checked throughout the experiment; more specifically,
484 the alkalinity and pH measured on aliquots at the reactor outlet showed values equivalent to
485 those obtained for SPW, i.e. between 2.1 and 2.4 meq L⁻¹ and 7.2-7.4, respectively. The Eu
486 concentration at the outlet of all reactors remained very low and stable over time, with average
487 values below 7×10^{-11} mol L⁻¹.

488

489 *III.3.1 Europium quantification at the surface of spiked samples (R1 and R2)*

490 The analyses of Eu concentrations carried out on the surface at the inlet side of samples are
491 given in Figure 5. The ablation depth by the laser beam was estimated at about 10 μm. The
492 average Eu concentration at the surface of spiked samples equals 47 ± 19 and 95 ± 32 μg g⁻¹
493 for R1 and R2, respectively (n = 9). Europium appears to be homogeneously distributed on the
494 inlet faces even though the uncertainties associated with the derived concentrations are quite
495 high.



496

497 *Fig. 5: Europium concentration at the surface of Eu-spiked CO_x samples for bulk material*
 498 *(R1 and R2) and clay fraction (R3). L stands for the ablation line number (average concentration over*
 499 *around 0.65 mm length).*

500

501 During dismantling, a few drops of the aqueous solution in the immediate vicinity of the inlet
 502 surface were collected, under pressure, in order to measure the Eu concentration as close as
 503 possible to the sample surface. This analysis showed a decrease by a factor of about 3 with
 504 respect to the concentration of injected solution ($8.8 \times 10^{-8} \text{ mol L}^{-1}$ initially), i.e. between 2.4×10^{-8}
 505 8 and $2.7 \times 10^{-8} \text{ mol L}^{-1}$. This decrease in concentration is not easily explained. Experiments

506 conducted with HTO do not indicate any significant dilution resulting from the solution
507 injection protocol (Fig. A5); moreover, the experimental set-up was designed to limit Eu
508 adsorption on the surface of the materials used.

509 Regardless of the reason (e.g. possible slight adsorption of Eu on the PEEK material of the
510 capillary loop), the measured concentrations injected into the CO_x sample constitute the data
511 required to revert to the R_d values. Considering that a non-transient state was reached at the
512 surface where pore water concentration corresponds to injected concentration, R_d values of
513 $11,500 \pm 5,000 \text{ L kg}^{-1}$ and $26,300 \pm 9,500 \text{ L kg}^{-1}$ were obtained for R1 and R2, respectively.
514 Although a factor of close to two lies between the values, they do agree, within the limits of
515 uncertainty, with the predicted range of R_d values, within which the adsorption data recorded
516 in the dispersed state all lie (open symbols in Fig. 3).

517

518 *III.3.2 Eu localization at the surface of the spiked sample R3*

519 Since no significant compaction effect was observed and given that the sorption model
520 satisfactorily predicts the experimental retention data, Eu was expected to be adsorbed by the
521 clay fraction. This outcome was assessed directly on the R3 sample. Note that for this reactor,
522 unlike reactors 1 and 2, the Eu concentration measured at the reactor inlet ($9.1 \pm 0.7 \cdot 10^{-8} \text{ mol L}^{-1}$)
523 corresponded to the Eu concentration injected into the loop.

524 The areas rich in clay were previously identified by optical microscopy. Several laser ablation
525 lines were carried out (see Fig. 5 for results). Note that the analysis of the major elements indeed
526 confirms that the clay fraction has been appropriately targeted (Fig. A6). As expected, the Eu
527 concentration measured in the clay matrix of the Eu-spiked CO_x sample ($[\text{Eu}]_{\text{clay,R3}}$) is clearly
528 higher than that for the natural CO_x ($[\text{Eu}]_{\text{clay,CO}_x}$), i.e. $311 \pm 62 \mu\text{g g}^{-1}$ vs. $1.2 \pm 0.5 \mu\text{g g}^{-1}$. In
529 taking into account the percentage of clay in the CO_x ($P_{\text{clay,CO}_x}$), as well as the concentration of
530 Eu injected into the compact system ($[\text{Eu}]_{\text{injected}}$), the molecular weight of Eu (MM_{Eu}) and the

531 fact that a non-transient state has been reached at the "interface", an Rd value can be calculated
532 according to the following:

$$533 \quad Rd = 10^{-3} \frac{([Eu]_{\text{clay,R3}} - [Eu]_{\text{clay,COx}}) P_{\text{clay,COx}}}{MM_{\text{Eu}} [Eu]_{\text{injected}}} \quad (6)$$

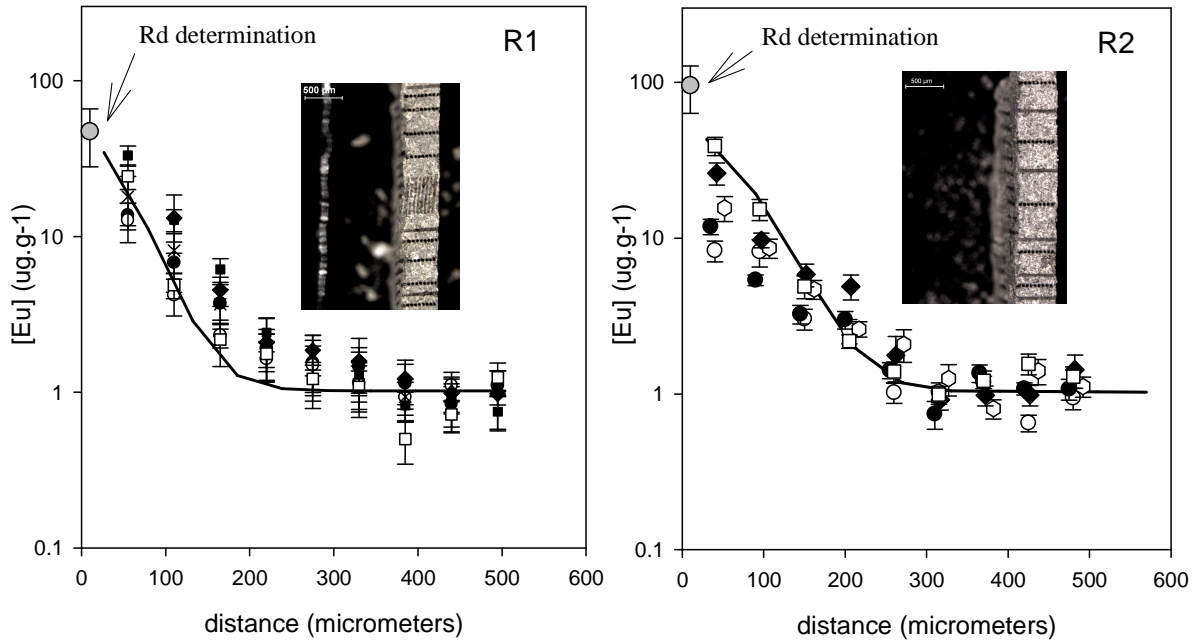
534 The Rd value obtained ($11,200 \pm 5,700 \text{ L kg}^{-1}$) also appears to be consistent with the retention
535 data previously determined for reactors R1 and R2 and with the values measured in the
536 dispersed state. These results are entirely consistent with the hypothesis that clay fraction
537 governs Eu adsorption.

538

539 *III.3.3 Europium concentration along the spiked COx samples*

540 In a final step, the Eu concentration was assessed along the samples as a function of depth for
541 both the R1 and R2 reactors. The "percolation depth profiles" obtained are shown in Figure 6;
542 let's note that although the profiles resemble one another, the data are rather scattered. As
543 expected, Eu reaches its highest concentrations within the first few micrometers ($< 50 \mu\text{m}$) of
544 the sample, even though migration was detected up to a depth of approx. $200 \mu\text{m}$. From a depth
545 of $200 \mu\text{m}$ and beyond, the geochemical background of Eu in COx is in fact being analyzed,
546 i.e. approx. $0.9 \mu\text{g g}^{-1}$.

547 The percolation profiles were then simulated by coupling the chemistry model applicable for
548 the Eu concentrations investigated (solid lines in Fig. 3, see Tables A2 and A3 for the
549 parameters) with an advective transport model (see Table A1 for detailed information). No
550 adjustment was attempted, as this multi-parametric model lacking constraints does not output
551 precise parameters. The simulation results (solid lines in the figure) are in good agreement with
552 experience, provided the trends are well reproduced.



553

554 *Fig. 6: Europium concentration along the COx sample for R1 (25 mL of percolated Eu-spiked SPW)*
 555 *and R2 (49 mL of percolated Eu-spiked SPW). The various series represent different laser ablation spot*
 556 *lines. The lines reflect simulations made with reactive transport model. The gray symbols correspond*
 557 *to the surface analysis ($\approx 10 \mu\text{m}$).*

558

559 **IV. Discussion**

560 With regard to the key question raised in this work, thanks to the proposed methodology, Rd
 561 values could be proposed to describe Eu adsorption on compact COx samples. The objective of
 562 this work has been to determine these values in a non-transient state, where the thermodynamic
 563 model can be directly applied without considering the transport part. This condition is
 564 anticipated at the sample surface after a certain contact time, when the pore water concentration
 565 corresponds to that of the injected solution (dashed zone in Fig. 1).

566 The contact time required to reach this non-transient state at the COx pellet entry surface has
 567 not been evaluated experimentally, as this step would have required excessive experimental
 568 work given the difficulty of setting up these experiments. In this context, the simulation results
 569 prove to be quite important. As revealed by the depth profile simulation results (Fig. 6), the
 570 level of agreement between experiment and calculation is satisfactory, especially when

571 considering that no parameters have been adjusted. A more detailed examination indicates that
572 the extrapolation of simulation curves out to the surface explored by laser ablation coincides
573 with the measured Eu concentration values. Recall that these measured values are the origin of
574 the experimental R_d values, which themselves are accurately reproduced by the chemical model
575 (Fig. 3). It can thus be concluded that simulations confirm that the experimental time was
576 sufficient to achieve the desired non-transient state at the interface for R1 and R2, as proposed
577 in our strategy. Since the percolated volume is even greater for R3, the conditions are therefore
578 logically applicable to this reactor as well.

579 Europium adsorption onto COx was shown to be strong ($R_d > 10^4 \text{ L kg}^{-1}$) at trace
580 concentrations. Similar behavior would be expected for the trivalent actinides Am and Cm, as
581 well for Pu under highly reducing conditions. Furthermore, the three R_d values obtained for the
582 compact spiked COx samples are consistent, within the experimental uncertainties, with those
583 deduced from conventional batch experiments carried out in dispersed state (black symbols in
584 Fig. 3). Similar results had already been obtained for compact COx with iodine (I) (Montavon
585 et al., 2014), cesium (Cs) (Chen et al., 2014b) and nickel (Ni) (Montavon et al., 2020), thus
586 suggesting that this trend seems *a priori* applicable to the retention of metal ions by COx clay
587 rock. The result also appears to be consistent with the recent results of Glaus et al. (2020),
588 derived from diffusion experiments vs. pH for an Eu/compacted illite system. They
589 demonstrated that adsorption models are valid for describing the equilibrium distribution of Eu
590 between aqueous solution and clay phase in the compacted state, provided an electrical double
591 layer is considered to describe the behavior of mobile species in the diffuse layer.

592 A combination of the various methods also leads to conclude that the clay fraction effectively
593 governs Eu adsorption. This finding has been indirectly confirmed by modeling the data; in
594 using a bottom-up approach along with the assumption that the clay fraction is responsible for
595 element adsorption on COx (Table A2), it was possible to explain experimental adsorption data

596 in the conditions chosen for the percolation experiments, during which both strong and weak
597 sites contribute to Eu adsorption. This finding was also validated by direct analysis on the
598 compact Eu-spiked sample (R3); the additional Eu is derived quantitatively, within
599 uncertainties, in the clay fraction. This result is in agreement with qualitative data already
600 published by Menut et al. (2006) on Eu-spiked COx samples obtained from a diffusion
601 experiment and Laser-Induced Breakdown Spectroscopy (LIBS) measurements.

602 The importance of the clay fraction in Eu retention also corroborates the results of the study
603 conducted with naturally-occurring Eu. The clay fraction represents the main reservoir, with
604 some 70% of the inventory of naturally-occurring Eu found at trace concentrations in the COx
605 ($\approx 0.9 \text{ mg kg}^{-1}$). Using this value and the natural pore water concentration of Eu, Rd values
606 ranging from 6.10^4 to 2.10^5 L kg^{-1} are determined. The domain in Rd values is consistent with
607 predictive simulations yet lies beyond the values potentially extrapolated from adsorption data
608 recorded at the trace scale (in dispersed state); the Rd values over such a range are assumed to
609 be constant ($\approx 3.5 \times 10^4 \text{ L kg}^{-1}$). However, adsorption is not the only process leading to metal
610 retention and one shall recall that the total content of Eu in the clay rock is larger than the
611 fraction bound to the clay phases. On the other hand, only a fraction of the retained Eu is labile
612 and has to be taken into account for the evaluation of the Rd to be compared with the laboratory
613 retention experiments. Other processes leading to non-labile species, such as incorporation of
614 metals into matrices, are likely to occur, in particular for the long times characteristic of
615 sedimentary rocks (e.g. COx) (McKinley and Alexander, 1993). This outcome was recently
616 shown for the Ni/COx system (Montavon et al., 2020), whereby only $\approx 13\%$ of the Ni found in
617 the rock appeared to be labile/adsorbed (and only 24% of Ni found in the clay fraction). The
618 proposed *in situ* range of Rd values ($\approx 6.10^4$ to 2.10^5 L kg^{-1}) therefore represents an upper limit,
619 which cannot be simply compared to Rd values measured in the laboratory over short time

620 periods. On the other hand, the deviation between prediction and experiment for equilibrium
621 Eu concentrations below $\approx 10^{-8}$ mol L⁻¹ still needs to be elucidated.

622

623 **V. Conclusion**

624 Thanks to our methodology, and the use of LA-ICP-MS, it was possible to derive Rd values for
625 Eu on compact COx samples under non-transient conditions, i.e. without considering the
626 transport process. Within the uncertainties present, these values are of the same order of
627 magnitude as those derived in the dispersed state for the aqueous concentration range explored
628 for both states ($\sim 3 \cdot 10^{-8}$ - 10^{-7} mol/L). From a mechanistic point of view, retention can be
629 described by the reversible adsorption of Eu on the surface of clays (illite and illite/smectite)
630 based on existing adsorption models (for equilibrium Eu concentrations above $\approx 10^{-8}$ mol L⁻¹)
631 through carbonate surface complexes with strong sites. This finding was also shown directly by
632 mapping on the compact spiked sample (R3); the additional Eu is found quantitatively, again
633 within uncertainties, in the clay fraction. The magnitude of the clay fraction in Eu retention is
634 also observed for naturally-occurring Eu, with about 70% of the inventory found in the latter.
635 However, only a portion of this natural Eu in the clay fraction seems to be present in labile
636 (reversible) form, thus suggesting the existence of other retention mechanisms capable of
637 leading to metal entrapment. Further studies would be needed to assess the impact of this
638 irreversible entrapment of Eu and of other trivalent elements in minerals for the long-term safety
639 of radioactive waste disposal sites. Yet even when ignoring this additional margin of safety, our
640 data clearly demonstrate the strong retention of trivalent elements on clay rock, which makes
641 them very little mobile in the COx formation.

642

643 **Acknowledgments**

644 The authors would like to thank Andra (GL CTEC), contributors to the "Chaire stockage" unit
645 (EDF, ORANO and Andra). This project has also received funding from the European Union's
646 Horizon 2020 research and innovation program under grant agreement No 847593
647 (EURAD/FUTURE).

648

649 **References**

650 Aertsens, M., De Cannière, P., Moors, H., 2003. Modelling of silica diffusion experiments
651 with ³²Si in Boom Clay, in: *Journal of Contaminant Hydrology*. Elsevier, pp. 117–129.
652 [https://doi.org/10.1016/S0169-7722\(02\)00140-7](https://doi.org/10.1016/S0169-7722(02)00140-7)

653 Altmann, S., Aertsens, M., Appelo, T., Bruggeman, C., Gaboreau, S., Glaus, M., Jacquier, P.,
654 Kupcik, T., Maes, N., Montoya, V., Rabung, T., Robinet, J.-C., Sovoye, S., Schaefer, T.,
655 Tournassat, C., Van Laer, L., Van Loon, L., 2014. Processes of cation migration in
656 clayrocks (CatClay) - Final Scientific Report (D1.6).

657 ANDRA, 2005a. *Évolution Phénoménologique Du Stockage Géologique*.
658 <https://www.andra.fr/cigeo/les-documents-de-reference#section-967>.

659 ANDRA, 2005b. Dossier 2005 Argile: Tome Architecture et gestion du stockage géologique.

660 André, M., Malmström, M.E., Neretnieks, I., 2009. Determination of sorption properties of
661 intact rock samples: New methods based on electromigration. *J. Contam. Hydrol.* 103,
662 71–81. <https://doi.org/10.1016/j.jconhyd.2008.09.006>

663 Bazer-Bachi, F., Tevissen, E., Descostes, M., Grenut, B., Meier, P., Simonnot, M.O., Sardin,
664 M., 2006. Characterization of iodide retention on Callovo-Oxfordian argillites and its
665 influence on iodide migration. *Phys. Chem. Earth* 31, 517–522.
666 <https://doi.org/10.1016/j.pce.2006.04.015>

667 Bradbury, M.H., Baeyens, B., 2011. Predictive sorption modelling of Ni(II), Co(II), Eu(III),
668 Th(IV) and U(VI) on MX-80 bentonite and Opalinus Clay: A “bottom-up” approach.
669 Appl. Clay Sci. 52, 27–33. <https://doi.org/10.1016/j.clay.2011.01.022>

670 Chen, Z., Montavon, G., Guo, Z., Wang, X., Razafindratsima, S., Robinet, J.C., Landesman,
671 C., 2014a. Approaches to surface complexation modeling of Ni(II) on Callovo-Oxfordian
672 clayrock. Appl. Clay Sci. 101, 369–380. <https://doi.org/10.1016/j.clay.2014.07.034>

673 Chen, Z., Montavon, G., Ribet, S., Guo, Z., Robinet, J.C., David, K., Tournassat, C.,
674 Grambow, B., Landesman, C., 2014b. Key factors to understand in-situ behavior of Cs in
675 Callovo-Oxfordian clay-rock (France). Chem. Geol. 387, 47–58.
676 <https://doi.org/10.1016/j.chemgeo.2014.08.008>

677 Davies, C.W., 1964. Ion association. J. Electrochem. Soc. 111, 85C.

678 Davis, J.A., Coston, J.A., Kent, D.B., Fuller, C.C., 1998. Application of the surface
679 complexation concept to complex mineral assemblages. Environ. Sci. Technol. 32,
680 2820–2828. <https://doi.org/10.1021/es980312q>

681 Descostes, M., Pointeau, I., Radwan, J., Poonoosamy, J., Lacour, J.L., Menut, D., Vercouter,
682 T., Dagnelie, R.V.H., 2017. Adsorption and retarded diffusion of EuIII-EDTA– through
683 hard clay rock. J. Hydrol. 544, 125–132. <https://doi.org/10.1016/j.jhydrol.2016.11.014>

684 García-Gutiérrez, M., Alonso, U., Missana, T., Cormenzana, J., Mingarro, M., Morejón, J.,
685 Gil, P., 2009. Diffusion Experiments with Opalinus and Callovo-Oxfordian Clays:
686 Laboratory, Large-Scale Experiments and Microscale Analysis by RBS. MADRID,
687 ESPAÑA.

688 Gaucher, E., Robelin, C., Matray, J.M., Négrel, G., Gros, Y., Heitz, J.F., Vinsot, A., Rebours,
689 H., Cassagnabère, A., Bouchet, A., 2004. ANDRA underground research laboratory:

690 Interpretation of the mineralogical and geochemical data acquired in the Callovian-
691 Oxfordian formation by investigative drilling. *Phys. Chem. Earth* 29, 55–77.
692 <https://doi.org/10.1016/j.pce.2003.11.006>

693 Gaucher, E.C., Tournassat, C., Pearson, F.J., Blanc, P., Crouzet, C., Lerouge, C., Altmann, S.,
694 2009. A robust model for pore-water chemistry of clayrock. *Geochim. Cosmochim. Acta*
695 73, 6470–6487. <https://doi.org/10.1016/j.gca.2009.07.021>

696 Giffaut, E., Grivé, M., Blanc, P., Vieillard, P., Colàs, E., Gailhanou, H., Gaboreau, S., Marty,
697 N., Madé, B., Duro, L., 2014. Andra thermodynamic database for performance
698 assessment: ThermoChimie. *Appl. Geochemistry* 49, 225–236.
699 <https://doi.org/10.1016/j.apgeochem.2014.05.007>

700 Glaus, M.A., Frick, S., Van Loon, L.R., 2020. A coherent approach for cation surface
701 diffusion in clay minerals and cation sorption models: Diffusion of Cs⁺ and Eu³⁺ in
702 compacted illite as case examples. *Geochim. Cosmochim. Acta* 274, 79–96.
703 <https://doi.org/10.1016/j.gca.2020.01.054>

704 Grambow, B., 2016. Geological disposal of radioactive waste in clay. *Elements* 12, 239–245.

705 Grangeon, S., Vinsot, A., Tournassat, C., Lerouge, C., Giffaut, E., Heck, S., Groschopf, N.,
706 Denecke, M.A., Wechner, S., Schäfer, T., 2015. The influence of natural trace element
707 distribution on the mobility of radionuclides. The exemple of nickel in a clay-rock. *Appl.*
708 *Geochemistry* 52, 155–173. <https://doi.org/10.1016/j.apgeochem.2014.11.009>

709 Grivé, M., Duro, L., Colàs, E., Giffaut, E., 2015. Thermodynamic data selection applied to
710 radionuclides and chemotoxic elements: An overview of the ThermoChimie-TDB. *Appl.*
711 *Geochemistry* 55, 85–94. <https://doi.org/10.1016/j.apgeochem.2014.12.017>

712 Hassan Loni, Y., David, K., Larrue, S., Grambow, B., Corona, C., Ribet, S., Chardon, P.,

713 Montavon, G., 2019. Uranium quantification of oak tree rings (*Quercus petraea*) from a
714 former uranium mining site by High Resolution Inductively Coupled Plasma Mass
715 spectrometry in Laser Ablation and Solution modes. *Spectrochim. Acta - Part B At.*
716 *Spectrosc.* 161, 105709. <https://doi.org/10.1016/j.sab.2019.105709>

717 Kasar, S., Kumar, S., Bajpai, R.K., Tomar, B.S., 2016. Diffusion of Na(I), Cs(I), Sr(II) and
718 Eu(III) in smectite rich natural clay. *J. Environ. Radioact.* 151, 218–223.
719 <https://doi.org/10.1016/j.jenvrad.2015.10.012>

720 Kautenburger, R., Beck, H.P., 2010. Influence of geochemical parameters on the sorption and
721 desorption behaviour of europium and gadolinium onto kaolinite. *J. Environ. Monit.* 12,
722 1295–1301. <https://doi.org/10.1039/b914861b>

723 Lerouge, C., Grangeon, S., Gaucher, E.C., Tournassat, C., Agrinier, P., Guerrot, C., Widory,
724 D., Fléhoc, C., Wille, G., Ramboz, C., Vinsot, A., Buschaert, S., 2011. Mineralogical
725 and isotopic record of biotic and abiotic diagenesis of the Callovian-Oxfordian clayey
726 formation of Bure (France). *Geochim. Cosmochim. Acta* 75, 2633–2663.
727 <https://doi.org/10.1016/j.gca.2011.02.025>

728 Lin, J., Liu, Y., Yang, Y., Hu, Z., 2016. Calibration and correction of LA-ICP-MS and LA-
729 MC-ICP-MS analyses for element contents and isotopic ratios. *Solid Earth Sci.* 1, 5–27.
730 <https://doi.org/10.1016/j.sesci.2016.04.002>

731 Liu, Y., Hu, Z., Gao, S., Günther, D., Xu, J., Gao, C., Chen, H., 2008. In situ analysis of
732 major and trace elements of anhydrous minerals by LA-ICP-MS without applying an
733 internal standard. *Chem. Geol.* 257, 34–43.
734 <https://doi.org/10.1016/j.chemgeo.2008.08.004>

735 Maes, N., Salah, S., Jacques, D., Aertsens, M., Van Gompel, M., De Cannière, P.,
736 Velitchkova, N., 2008. Retention of Cs in Boom Clay: Comparison of data from batch

737 sorption tests and diffusion experiments on intact clay cores. *Phys. Chem. Earth* 33,
738 S149–S155. <https://doi.org/10.1016/j.pce.2008.10.002>

739 Marques Fernandes, M., Vér, N., Baeyens, B., 2015. Predicting the uptake of Cs, Co, Ni, Eu,
740 Th and U on argillaceous rocks using sorption models for illite. *Appl. Geochemistry* 59,
741 189–199. <https://doi.org/10.1016/j.apgeochem.2015.05.006>

742 McKinley, I.G., Alexander, W.R., 1993. Assessment of radionuclide retardation: realistic
743 application of natural analogue studies. *J. Contam. Hydrol.* 13, 249–259.

744 Menut, D., Descostes, M., Meier, P., Radwan, J., Patrick, M., Poinssot, C., 2006. Europium
745 migration in Argillaceous Rocks : on the use of Micro Laser-Induced Breakdown
746 Spectroscopy (micro LIBS) as a Microanalysis Tool. *Mater. Res. Soc.* 932, 3–9.

747 Miller, A.W., Wang, Y., 2012. Radionuclide interaction with clays in dilute and heavily
748 compacted systems: A critical review. *Environ. Sci. Technol.* 46, 1981–1984.
749 <https://doi.org/10.1021/es203025q>

750 Molera, M., Eriksen, T., 2002. Diffusion of $^{22}\text{Na}^+$, $^{85}\text{Sr}^{2+}$, $^{134}\text{Cs}^+$ and $^{57}\text{Co}^{2+}$ in bentonite
751 clay compacted to different densities: Experiments and modeling. *Radiochim. Acta* 90,
752 753–760. https://doi.org/10.1524/ract.2002.90.9-11_2002.753

753 Monnier, L., Lach, P., Salvi, S., Melleton, J., Bailly, L., Béziat, D., Monnier, Y., Gouy, S.,
754 2018. Quartz trace-element composition by LA-ICP-MS as proxy for granite
755 differentiation, hydrothermal episodes, and related mineralization: The Beauvoir Granite
756 (Echassières district), France. *Lithos* 320–321, 355–377.
757 <https://doi.org/10.1016/j.lithos.2018.09.024>

758 Montavon, G., Lerouge, C., David, K., Ribet, S., Hassan-Loni, Y., Leferrec, M., Bailly, C.,
759 Robinet, J.-C., Grambow, B., 2020. Nickel Retention on Callovo-Oxfordian Clay:

760 Applicability of Existing Adsorption Models for Dilute Systems to Real Compact Rock.
761 Environ. Sci. Technol. <https://doi.org/10.1021/acs.est.0c04381>

762 Montavon, G., Sabatié-Gogova, A., Ribet, S., Bailly, C., Bessaguet, N., Durce, D., Giffaut, E.,
763 Landesman, C., Grambow, B., 2014. Retention of iodide by the Callovo-Oxfordian
764 formation: An experimental study. *Appl. Clay Sci.* 87, 142–149.
765 <https://doi.org/10.1016/j.clay.2013.10.023>

766 Oscarson, D.W., 1994. Surface diffusion: Is it an important transport mechanism in
767 compacted clays? *Clays Clay Miner.* 42, 534–543.
768 <https://doi.org/10.1346/CCMN.1994.0420504>

769 Parkhurst, D.L., Appelo, C.A.J., 2013. Description of input and examples for PHREEQC
770 version 3: a computer program for speciation, batch-reaction, one-dimensional transport,
771 and inverse geochemical calculations, *Techniques and Methods*. Reston, VA.
772 <https://doi.org/10.3133/tm6A43>

773 Schott, J., Acker, M., Barkleit, A., Brendler, V., Taut, S., Bernhard, G., 2012. The influence
774 of temperature and small organic ligands on the sorption of Eu(III) on Opalinus Clay.
775 *Radiochim. Acta* 100, 315–324. <https://doi.org/10.1524/ract.2012.1921>

776 Šelih, V.S., Van Elteren, J.T., 2011. Quantitative multi-element mapping of ancient glass
777 using a simple and robust LA-ICP-MS rastering procedure in combination with image
778 analysis. *Anal. Bioanal. Chem.* 401, 745–755. [https://doi.org/10.1007/s00216-011-5119-](https://doi.org/10.1007/s00216-011-5119-8)
779 8

780 Sellin, P., Leupin, O.X., 2013. The use of clay as an engineered barrier in radioactive-waste
781 management - A review. *Clays Clay Miner.* 61, 477–498.
782 <https://doi.org/10.1346/CCMN.2013.0610601>

783 Tournassat, C., Lerouge, C., Blanc, P., Brendlé, J., Greneche, J.M., Touzelet, S., Gaucher,
784 E.C., 2008. Cation exchanged Fe(II) and Sr compared to other divalent cations (Ca, Mg)
785 in the bure Callovian-Oxfordian formation: Implications for porewater composition
786 modelling. *Appl. Geochemistry* 23, 641–654.
787 <https://doi.org/10.1016/j.apgeochem.2007.11.002>

788 Van Elteren, J.T., Tennent, N.H., Šelih, V.S., 2009. Multi-element quantification of
789 ancient/historic glasses by laser ablation inductively coupled plasma mass spectrometry
790 using sum normalization calibration. *Anal. Chim. Acta* 644, 1–9.
791 <https://doi.org/10.1016/j.aca.2009.04.025>

792 Van Loon, L.R., Baeyens, B., Bradbury, M.H., 2009. The sorption behaviour of caesium on
793 Opalinus Clay: A comparison between intact and crushed material. *Appl. Geochemistry*
794 24, 999–1004. <https://doi.org/10.1016/j.apgeochem.2009.03.003>

795 Van Loon, L.R., Baeyens, B., Bradbury, M.H., 2005. Diffusion and retention of sodium and
796 strontium in Opalinus clay: Comparison of sorption data from diffusion and batch
797 sorption measurements, and geochemical calculations. *Appl. Geochemistry* 20, 2351–
798 2363. <https://doi.org/10.1016/j.apgeochem.2005.08.008>

799 Van Loon, L.R., Glaus, M.A., 2008. Mechanical compaction of smectite clays increases ion
800 exchange selectivity for cesium. *Environ. Sci. Technol.* 42, 1600–1604.
801 <https://doi.org/10.1021/es702487m>

802 Vinsot, A., Mettler, S., Wechner, S., 2008. In situ characterization of the Callovo-Oxfordian
803 pore water composition. *Phys. Chem. Earth* 33.
804 <https://doi.org/10.1016/j.pce.2008.10.048>

805 Wang, X., Chen, Y., Wu, Y., 2004. Diffusion of Eu(III) in compacted bentonite - Effect of
806 pH, solution concentration and humic acid. *Appl. Radiat. Isot.* 60, 963–969.

807 <https://doi.org/10.1016/j.apradiso.2004.01.008>

808